Urinary secretion and extracellular aggregation of mutant uromodulin isoforms

Céline Schaeffer[1,2], Angela Cattaneo[2], Matteo Trudu[1,2], Sara Santambrogio[1,2,9], Ilenia Bernascone[1,2,10], Daniela Giachino[3], Gianluca Caridi[4], Andrea Campo[5], Corrado Murtas[6], Simona Benoni[3], Claudia Izzi[7], Mario De Marchi[3], Antonio Amoroso[8], Gian Marco Ghiggeri[4], Francesco Scolari[7], Angela Bachi[2] and Luca Rampoldi[1,2]

[1]Dulbecco Telethon Institute, San Raffaele Scientific Institute, Milan, Italy; [2]Division of Genetics and Cell Biology, San Raffaele Scientific Institute, Milan, Italy; [3]Department of Clinical and Biological Sciences, University of Turin, Turin, Italy; [4]Division of Nephrology, G Gaslini Institute, Genoa, Italy; [5]SOC Nefrologia, Dialisi e Nutrizione Clinica, Presidio Ospedaliero San Lazzaro di Alba, Cuneo, Italy; [6]Department of Clinical Medicine, Nephrology and Health Sciences, University of Parma, Parma, Italy; [7]Division of Nephrology, Montichiari Hospital, Brescia, Italy and [8]Department of Genetics, Biology and Biochemistry, University of Turin, Turin, Italy

Uromodulin is exclusively expressed in the thick ascending limb and is the most abundant protein secreted in urine where it is found in high-molecular-weight polymers. Its biological functions are still elusive, but it is thought to play a protective role against urinary tract infection, calcium oxalate crystal formation, and regulation of water and salt balance in the thick ascending limb. Mutations in uromodulin are responsible for autosomal-dominant kidney diseases characterized by defective urine concentrating ability, hyperuricemia, gout, tubulointerstitial fibrosis, renal cysts, and chronic kidney disease. Previous *in vitro* studies found retention in the endoplasmic reticulum as a common feature of all uromodulin mutant isoforms. Both *in vitro* and *in vivo* we found that mutant isoforms partially escaped retention in the endoplasmic reticulum and reached the plasma membrane where they formed large extracellular aggregates that have a dominant-negative effect on coexpressed wild-type protein. Notably, mutant uromodulin excretion was detected in patients carrying uromodulin mutations. Thus, our results suggest that mutant uromodulin exerts a gain-of-function effect that can be exerted by both intra- and extracellular forms of the protein.

Kidney International (2012) **81,** 769–778; doi:10.1038/ki.2011.456; published online 11 January 2012

KEYWORDS: aggregation; Tamm–Horsfall protein; urinary protein secretion; uromodulin

Correspondence: *Luca Rampoldi, Dulbecco Telethon Institute c/o Molecular Genetics of Renal Disorders, Division of Genetics and Cell Biology, San Raffaele Scientific Institute, Via Olgettina 58, 20132 Milan, Italy. E-mail: rampoldi.luca@hsr.it*

[9]Current address: Institute of Physiology, University of Zurich, Zurich, Switzerland.

[10]Current address: Centro de Biologia Molecular Severo Ochoa, Madrid, Spain.

Received 21 April 2011; revised 5 October 2011; accepted 25 October 2011; published online 11 January 2012

Uromodulin, also known as Tamm–Horsfall protein, was discovered in 1950 by Tamm and Horsfall.[1] It is a large glycoprotein of ~105 kDa that is exclusively expressed in the kidney in the thick ascending limb (TAL) of Henle's loop. Uromodulin is a glycosylphosphatidylinositol-anchored protein mainly localized at the apical plasma membrane of epithelial tubular cells,[2] from which it is released into the tubular lumen through a proteolytic cleavage by a yet to be identified protease.[3] In the urine, it constitutes the most abundant protein and it is mainly found as a high-molecular-weight polymer (Mr 1–10 × 10^6).[4]

Mutations in the *UMOD* gene encoding uromodulin have been shown to cause medullary cystic kidney disease type 2 (Online Mendelian Inheritance in Man (OMIM) 603860), familial juvenile hyperuricemic nephropathy (OMIM 162000),[5] and glomerulocystic kidney disease with hyperuricemia (OMIM 609886),[6,7] collectively referred to as uromodulin-associated kidney diseases (UAKD). UAKD are autosomal-dominant disorders characterized by alteration of urinary concentrating ability and by tubulointerstitial fibrosis, hyperuricemia, and gout, and in few cases by renal cysts at the corticomedullary junction.[8] Although UAKD are heterogeneous in terms of age at onset, clinical features, and presence of cysts, they invariably lead to chronic kidney disease during the third to fifth decade of life.

To date, 51 mutations have been described. All but three (in-frame deletions) are missense changes that are clustered in the N-terminal half of the protein. *In vitro* studies performed in diverse cell lines have shown that mutant uromodulin isoforms are defective in trafficking to the plasma membrane and are retained in the endoplasmic reticulum (ER).[9–12] Enrichment and aggregation of mutant uromodulin in the ER have been confirmed in a transgenic mouse model that we recently reported and in patient biopsies.[10,13] All together, these results suggest ER retention of mutant uromodulin as a key primary event in UAKD

pathogenesis. Interestingly, both *in vitro* and *in vivo* models show that mutant uromodulin can in part reach the plasma membrane carrying mature, post-ER type of glycans.[9,10,13]

In this study, we investigate the effect of mutant uromodulin escaping ER quality control. We show that in both *in vitro* and *in vivo* models it forms aggregates at the plasma membrane and in the tubule lumen. Moreover, we provide novel evidence supporting that these changes in the extracellular compartment might be relevant in the human disease, as we identified mutant uromodulin secretion in urine samples from UAKD patients. All together, our data suggest the possibility of an extracellular gain of function and dominant-negative effect of mutant uromodulin isoforms.

RESULTS

Mutant uromodulin is trafficked to and aggregates at the plasma membrane

We investigated if mutant uromodulin can partially escape quality control in the ER and is trafficked to the plasma membrane. To do so, wild-type and mutant (R212C, C256Y, and C317Y) human uromodulin isoforms were stably expressed in MDCK (Madin–Darby canine kidney) cells. The C317Y mutation was previously reported and partially characterized *in vitro*.[6,14] Uromodulin mutations R212C and C256Y are novel and were identified after genetic screening in Italian UAKD families (Figure 1a and b). Similar to previous studies on uromodulin mutants, all analyzed mutations lead to partial ER retention of mutant protein (Figure 2a and b). Interestingly, wild-type protein reaching the plasma membrane assembles into polymeric filaments as described for urinary protein[15] (Figure 3). Although less efficiently, all mutant isoforms were also trafficked to the plasma membrane and secreted in the culturing medium. Notably, mutant protein is unable to assemble into ordered filaments but rather forms large aggregates on the plasma membrane. Mutant uromodulin, reaching the plasma membrane and released by phospholipase C (PLC) digestion, carries mature post-ER glycosylation, demonstrating that it escaped the ER quality control and entered the secretory pathway (Supplementary Figure S1 online).

Dominant-negative effect of extracellular mutant uromodulin on the polymerization of the wild-type isoform

To verify if aggregation of mutant uromodulin isoforms on the plasma membrane could be detrimental for the polymerization of the wild-type one, wild-type and mutant proteins were stably coexpressed in MDCK cells, mimicking the patient heterozygous state. Equal expression level of the two isoforms was ensured by using a bicistronic expression vector. On western blot, coexpression of both isoforms did not alter the band pattern that was observed when wild type and mutants were expressed alone and it did not affect the secretion of the wild type protein (Supplementary Figure S2 online). This shows that despite ER retention of mutant protein, trafficking of the coexpressed wild-type one is not altered or at least not to an extent that can be detected in our experiments. Interestingly, immunofluorescence analysis of nonpermeabilized cells shows that mutant protein reaching the plasma membrane colocalizes with the wild-type one in shortened and less structured polymers when compared with cells expressing wild-type protein only (Figure 4a). This was confirmed by the quantification of the average area of filament clusters (Figure 4b) as well as by differential migration on sucrose gradient (Figure 5). Indeed, sedimentation of wild-type protein polymers into higher density

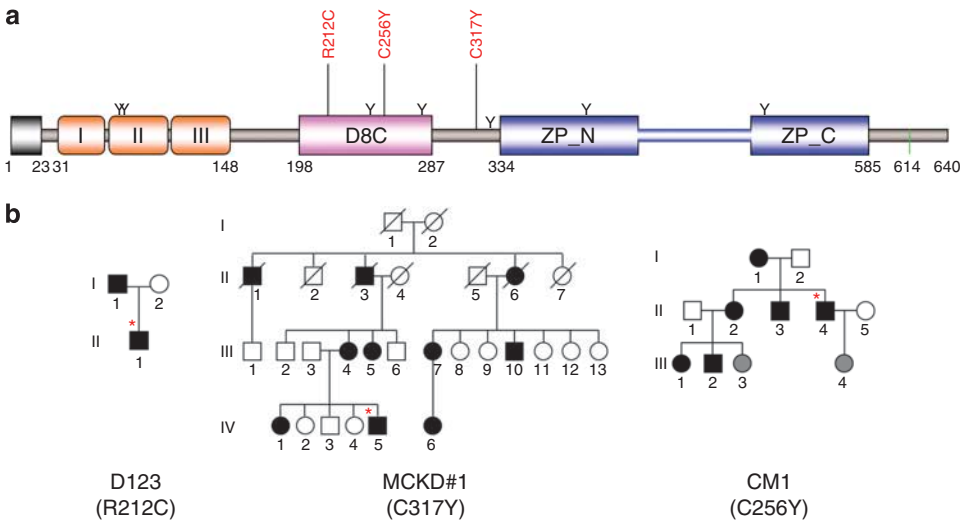

Figure 1 | Localization of the studied mutations and pedigree charts of the investigated families. (**a**) Schematic representation of uromodulin. The three epidermal growth factor (EGF) domains are represented by orange boxes, the D8C domain by a pink box, and the zona pellucida (ZP) domain (composed of ZP_N and ZP_C subdomains) is represented in blue. The glycosylphosphatidylinositol (GPI)-anchoring site as well as the glycosylation sites (Y) are shown. Studied mutations are indicated in red. (**b**) Pedigree charts of the three families D123, MCKD1, and CM1 bearing uromodulin mutations R212C, C256Y, and C317Y, respectively. *Urine mass spectrometry analysis.

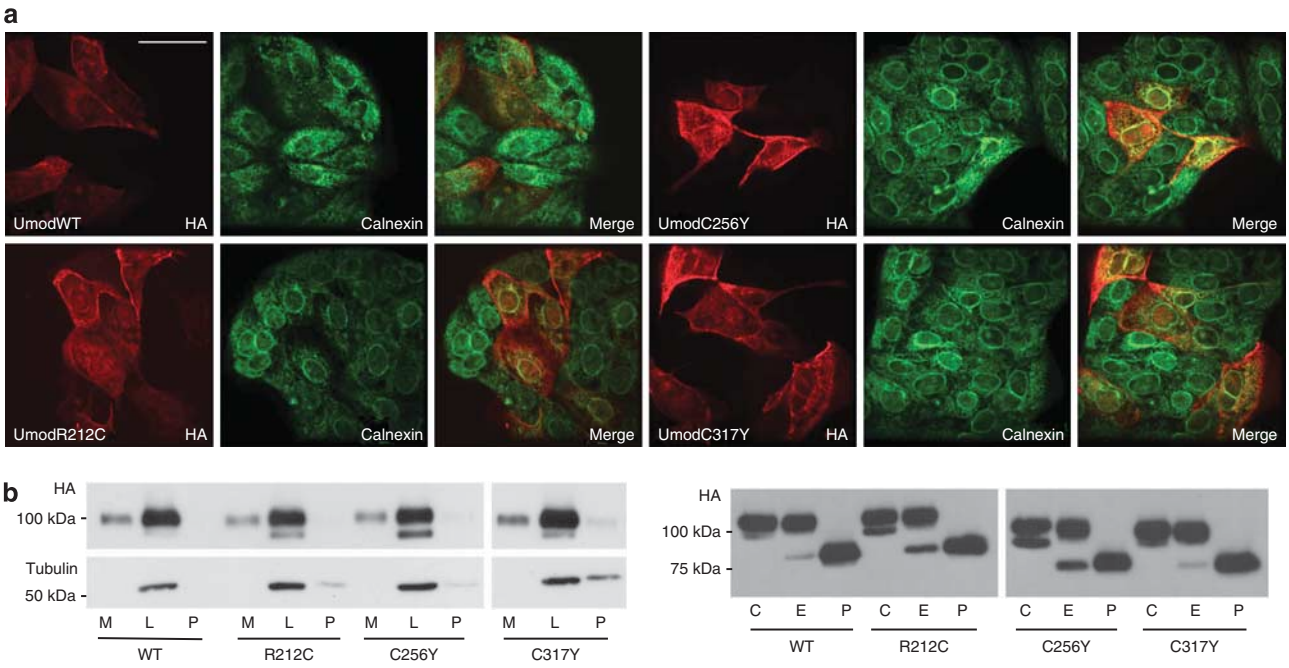

Figure 2 | Analysis of the trafficking of uromodulin isoforms. (**a**) Immunofluorescence analysis showing uromodulin in permeabilized MDCK (Madin–Darby canine kidney) cells stably expressing hemagglutinin (HA)-tagged wild-type (WT) or mutant uromodulin isoforms. Calnexin is shown as an endoplasmic reticulum (ER) marker. Bar = 35 μm. (**b**) Western blot detection of HA-tagged wild-type uromodulin or indicated mutants from the medium (M) and the soluble (L) and unsoluble (P) fractions of protein extracts from stably transfected MDCK cells. Tubulin is shown as a loading control (left panel). Western blot detection of uromodulin present in the cell lysate after deglycosylation with endoglycosidase H (EndoH; E) or peptide-N-glycosidase F (PNGase F; P); C, untreated sample (right panel).

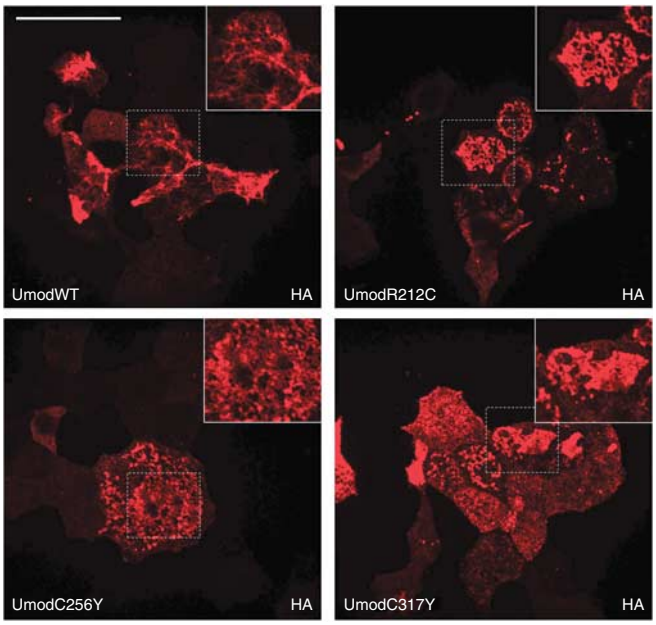

Figure 3 | Immunofluorescence showing uromodulin distribution on the plasma membrane in unpermeabilized MDCK (Madin–Darby canine kidney) cells stably expressing hemagglutinin (HA)-tagged wild-type (WT) or mutant uromodulin isoforms. Wild-type isoform is mainly present as large polymeric filaments whereas mutant isoforms form extracellular bulky aggregates. Bar = 35 μm.

fractions suggests that they are larger than the ones containing mutant isoforms also.[16] This effect is mediated by co-assembly of the two isoforms as demonstrated by co-immunoprecipitation of secreted wild-type and mutant uromodulin (Figure 6). Taken together, these results demonstrate that mutant uromodulin isoforms that reach the plasma membrane exert an extracellular dominant-negative effect on wild-type protein polymerization.

Mutant uromodulin is secreted in the urine of a transgenic mouse model of UAKD and forms intraluminal casts

We verified whether mutant uromodulin could indeed escape ER retention and form extracellular aggregates *in vivo* in a transgenic (Tg) mouse model of UAKD ($Tg^{UmodC147W}$) that expresses hemagglutinin (HA)-tagged mutant uromodulin (C147W),[13] corresponding to the patient mutation C148W that we already characterized *in vitro*.[6,9] As a first evidence of mutant uromodulin trafficking to the plasma membrane, we detected its presence in the urine of 12-week-old $Tg^{UmodC147W}$ mice. At this age, secretion of transgenic uromodulin is similar to the one in expression-matched mice transgenic for HA-tagged wild-type uromodulin (Tg^{Umodwt}; Figure 7a). Interestingly, urinary mutant uromodulin migrates slightly slower than the wild-type one on sodium dodecyl sulfate–polyacrylamide gel electrophoresis (SDS–PAGE). This size difference is eliminated by peptide-

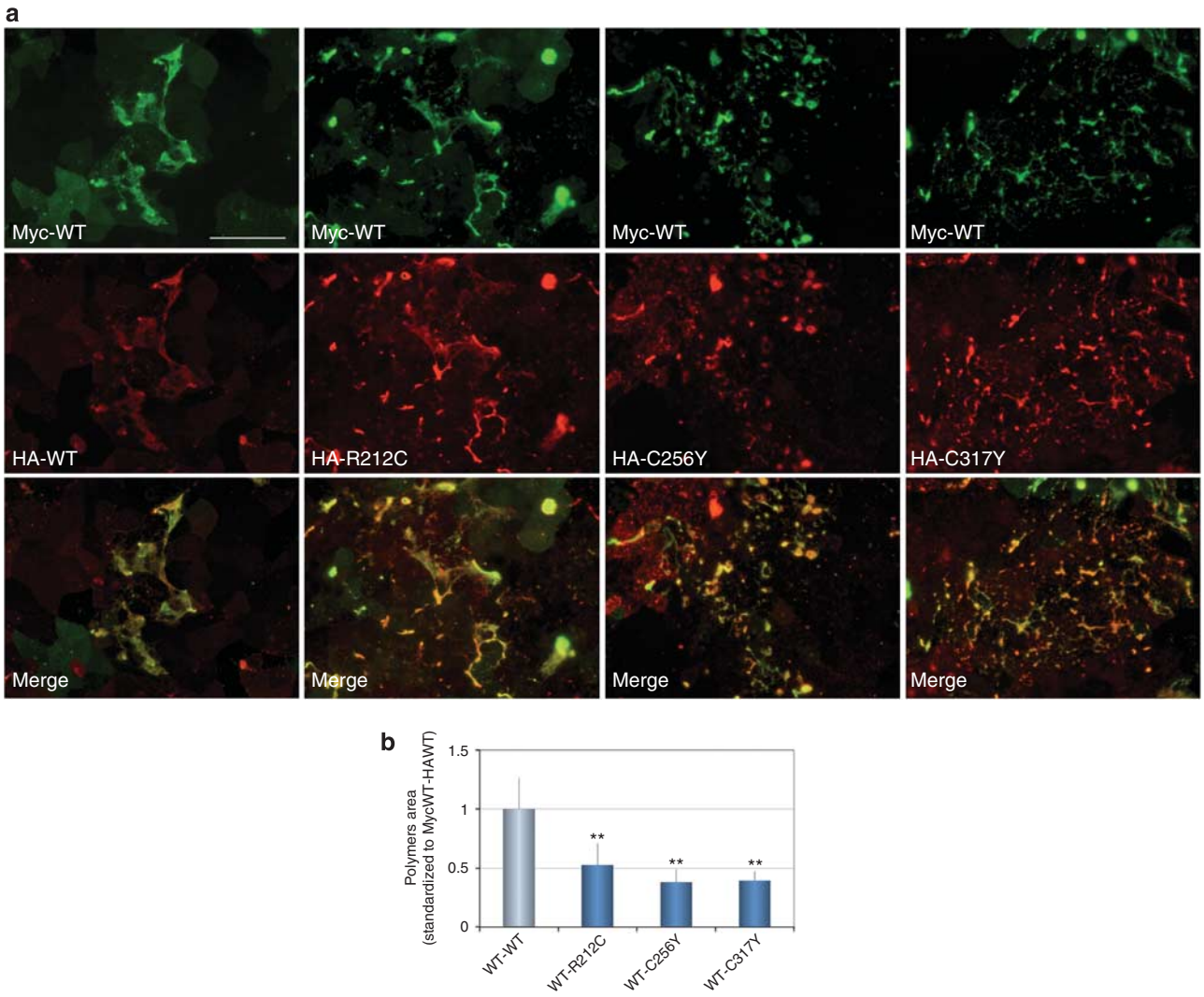

Figure 4 | Mutant uromodulin interferes with the polymerization of the wild-type isoform. (**a**) Immunofluorescence analysis showing uromodulin on the plasma membrane of unpermeabilized MDCK (Madin–Darby canine kidney) cells stably expressing myc-tagged wild-type (WT) isoform and either wild-type or mutant hemagglutinin (HA)-tagged isoforms. Staining with anti-HA and anti-myc antibodies is shown. The presence of the mutant isoform at the plasma membrane interferes with the polymerization of the wild-type one, as polymers look shortened and more aggregated. Bar = 55 μm. (**b**) Quantification of the average surface of uromodulin polymers on the membrane of MDCK cells coexpressing HA- and myc-tagged uromodulin isoforms. Only polymers containing co-transfected isoforms (positive for both tags) were quantified (~1000 counts per cell line per experiment, 2 independent experiments). Filaments formed by wild-type and mutant protein are significantly shortened. $^{**}P < 0.001$.

N-glycosidase F (PNGase F) digestion, suggesting that the two isoforms carry different *N*-glycosylation. Immunofluorescence performed on mouse kidney sections confirms the presence of extracellular mutant uromodulin in the lumen of TAL tubules. Similar to what is observed *in vitro*, mutant protein tends to form aggregates that are never observed in Tg^{Umodwt} mice (Figure 7b and c).

Mutant uromodulin is secreted in the urine of UAKD patients

We assessed the relevance of our *in vitro* and *in vivo* observations by investigating whether secretion of mutant uromodulin could also be observed in UAKD patients. We analyzed the secretion of mutant uromodulin in three patients bearing different uromodulin mutations (R212C, C256Y, or C317Y; Figure 1a) and with preserved renal function (Table 1). Mass spectrometry (MS) analyses show that in all cases, mutant isoforms are secreted in urine (Supplementary Figures S3–S5 online). Because summed peptide intensity can be used as a good proxy for absolute protein abundance,[17] the intensity signals of peptides specifically assigned to the wild-type protein were compared with the intensity signals of peptides specifically assigned to the mutant proteins, whereas signal intensities of common peptides of both isoforms were not considered. This method was used to have an estimate of the abundance of the urinary wild-type and mutant uromodulin isoforms in each patient. The ratio of the summed intensities of the specific peptides belonging to each uromodulin form is reported in Table 2.

The secretion of mutant isoforms R212C, C256Y, and C317Y was estimated to represent ~1.3%, 7.6%, and 35%, respectively, of the wild-type one.

DISCUSSION

To date, 51 mutations in the *UMOD* gene coding for uromodulin have been described, all leading to UAKD. Previous *in vitro* studies have pointed at ER retention as a common feature of all investigated mutants.[9–12] This was confirmed in a recently generated UAKD mouse model and on patient renal biopsy analysis.[10,13] All together, these data led to propose that mutant uromodulin intracellular aggregation could play a key role in the pathogenesis of the disease, likely by exerting a gain-of-function effect through activation of cell stress responses.

In this study, through *in vitro* and *in vivo* analyses we demonstrate that a part of mutant protein can escape the ER quality control, is trafficked to the plasma membrane, and secreted. Interestingly, mutant protein tends to form large extracellular aggregates that interfere with wild-type protein polymerization, suggesting extracellular gain of toxic function as an additional consequence of uromodulin mutations.

This effect was clearly evident in *in vitro* studies that were carried out in MDCK cells, which, to our knowledge, are the only cell models able to induce proper uromodulin polymerization into highly ordered filaments. This allowed us to show that mutant isoforms are unable to polymerize but rather form aggregates at the plasma membrane. Moreover, when wild-type and mutant uromodulin were coexpressed at equal levels, thereby mimicking the patient condition, we observed that mutant protein co-assembles with the wild-type one and exerts a dominant-negative effect over polymer formation and/or stability. Indeed, the presence of the mutant protein significantly shortens the polymers, as demonstrated by their quantification in immunofluorescence and their differential sedimentation on sucrose gradient. The dominant-negative effect on protein polymerization suggests that even if mutant protein has escaped the ER quality

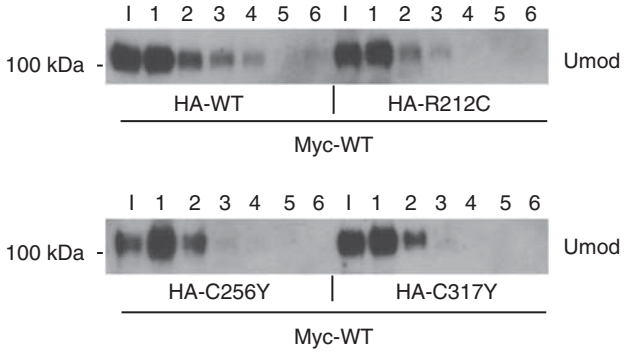

Figure 5 | Western blot analysis after separation on sucrose gradient of uromodulin digested by phosphatidylinositol-specific phospholipase C (PI-PLC) from MDCK (Madin–Darby canine kidney) cells expressing the myc-tagged wild-type (WT) isoform and either wild-type or mutant hemagglutinin (HA)-tagged isoforms. Fraction numbers are indicated from the top (1 M sucrose, fraction 1) to the bottom (2 M sucrose, fraction 6) of the gradient. I, input (1/5 of the amount loaded on the gradient). Uromodulin sediments deeper in the gradient when wild-type protein is expressed alone.

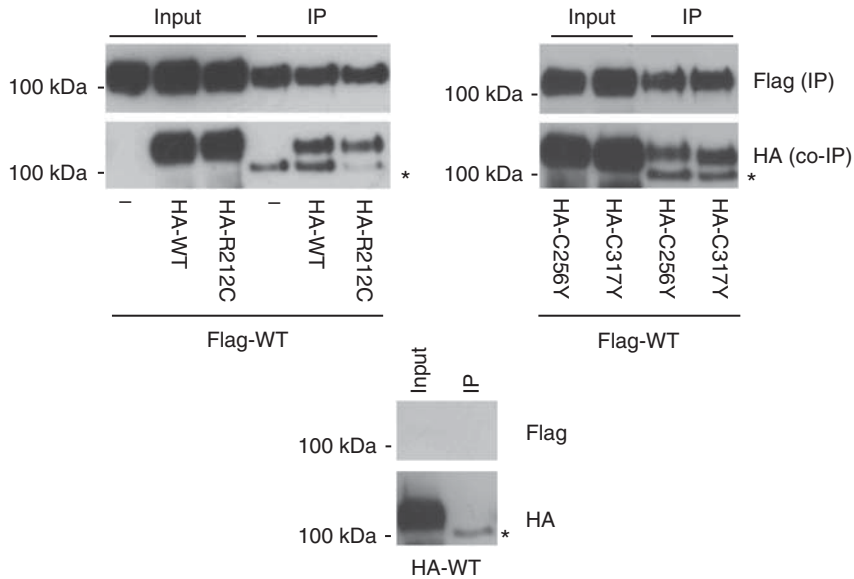

Figure 6 | Mutant uromodulin isoforms interact with the wild-type one. (Top panel) Co-immunoprecipitation (co-IP) experiments on protein from the conditioned medium of MDCK (Madin–Darby canine kidney) cells coexpressing Flag-tagged wild-type (WT) and hemagglutinin (HA)-tagged uromodulin isoforms. Immunoprecipitation was carried out with an anti-Flag antibody. The presence of co-immunoprecipitated HA-tagged uromodulin was assessed by western blot analysis. Mutant uromodulin co-assembles with wild-type protein. (Bottom panel) Same experiment performed on protein from the conditioned medium of MDCK cells expressing HA-tagged wild-type uromodulin isoform. The absence of co-immunoprecipitated HA-tagged uromodulin in the absence of Flag-tagged isoform demonstrates the specificity of the assay. *Unspecific signal. IP, immunoprecipitate.

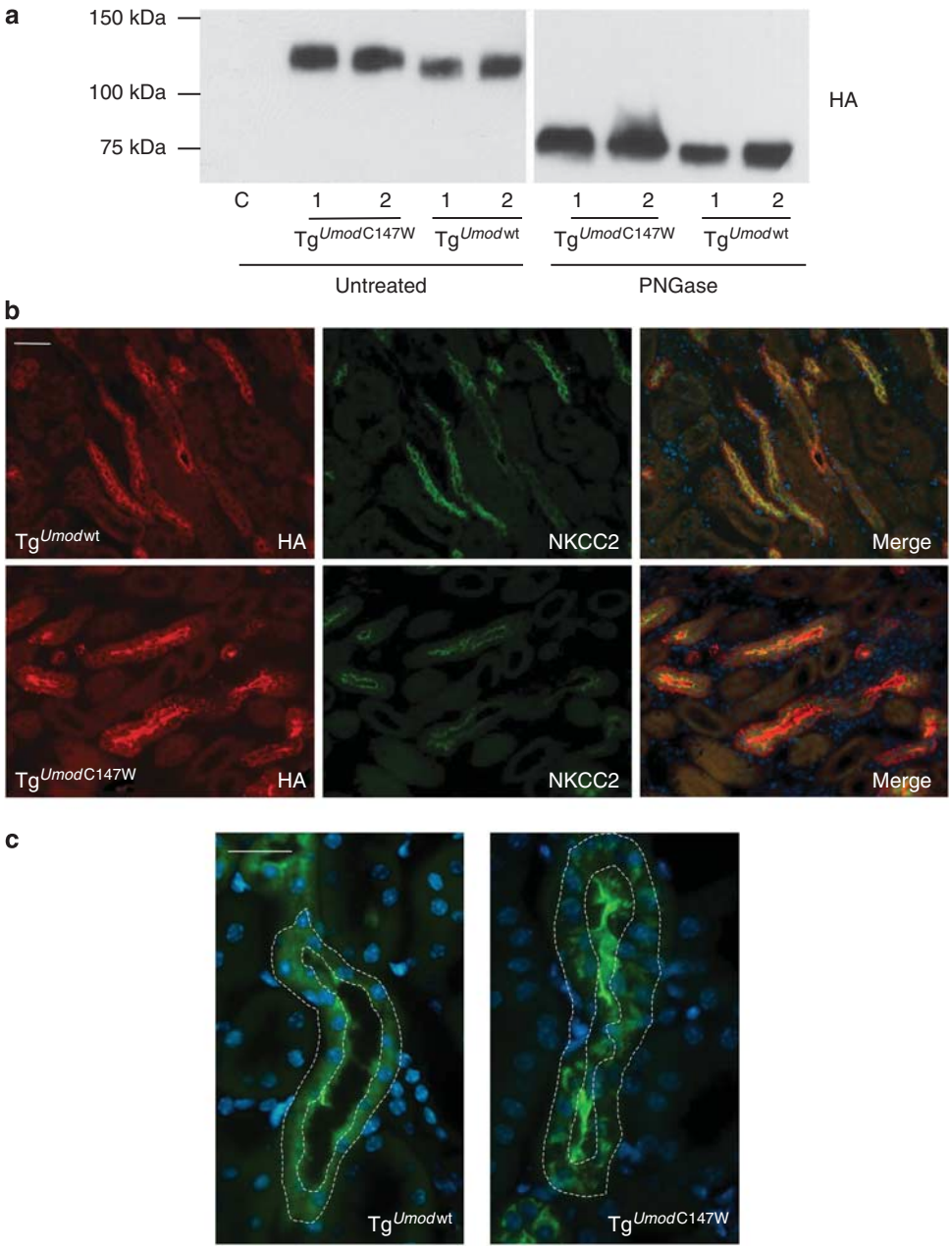

Figure 7 | Mutant uromodulin is secreted and forms intraluminal casts in a mouse model of UAKD. (**a**) Transgenic (Tg) hemagglutinin (HA)-tagged uromodulin secreted in the urine of Tg^{Umodwt} and $Tg^{UmodC147W}$ mice was analyzed by western blot. The amount of urine loaded is representative of a 24-h urine collection. Urinary uromodulin was also analyzed after deglycosylation with peptide-N-glycosidase F (PNGase F). (**b**) Immunofluorescence performed on kidney sections of Tg^{Umodwt} and $Tg^{UmodC147W}$ mice showing transgenic uromodulin and NKCC2 (apical marker of thick ascending limb (TAL) epithelial cells). Uromodulin aggregates are present exclusively in TAL lumen of $Tg^{UmodC147W}$ mice. Bar = 50 μm. (**c**) Immunofluorescence showing at higher magnification uromodulin aggregates present in TAL lumen of $Tg^{UmodC147W}$ mice and absent in Tg^{Umodwt} mice. Bar = 50 μm. C, control nontransgenic animal.

Table 1 | Summary of clinical features in the UAKD patients analyzed

Uromodulin mutation	Patient	Sex	Age at urine collection	Urine-specific gravity	Urinary creatinine (mg/dl)	Serum creatinine (mg/dl)	Serum uric acid (mg/dl)	Gout	Renal ultrasound
R212C	II 1	M	41	1010	65.5	1.08	6.2	No	NK
C256Y	II 4	M	35	1018	73	1.4	8.9	No	NK
C317Y	IV 5	M	18	1020	80	0.8	7.5	No	NK

Abbreviations: M, male; NK, normal kidney; UAKD, uromodulin-associated kidney diseases.

Table 2 | Intensities of specific peptides belonging to wild-type and mutant uromodulin isoforms as detected in urine samples from UAKD patients and calculation of their relative abundance

Sequence	Mass	Accession number	PEP	Intensity sample	The wt/mutant peptide intensity	%Mutant vs. wt
Patient II-1 (R212C)						
FVGQGGA**C**MAETCVPVLR	1836	IPI99999999	2.843E–3	703,400	76.3	1.3%
FVGQGGAR	790	IPI00013945	9.630E–3	231,460		
MAETCVPVLR	1117	IPI00013945	5.089 E–3	53,459,000		
Patient II-4 (C256Y)						
ACAHWSGHCCLWDASVQVK	2099	IPI00013945	7.90E–11	293,380,000	13.12	7.6%
ACAHWSGHC**Y**LWDASVQVK	2159	IPI99999996	3.85E–08	29,253,000		
KACAHWSGHCCLWDASVQVK	2228	IPI00013945	1.03E–14	90,289,000		
Patient IV-5 (C317Y)						
WHCQCK	803	IPI00013945	0.39716	2,342,100	2.80	35.7%
WHCQCKQDFNITDISLLEHR	2485	IPI00013945	6.92E–08	3,591,500		
WHCQ**Y**KQDFNITDISLLEHR	2545	IPI99999995	0.036102	2,434,900		
SNNGRWHCQCK	1331	IPI00013945	0.011313	281,370		
SNNGRWHCQCKQDFNITDISLLEHR	3013	IPI00013945	0.025424	598,510		

Abbreviations: Mass, mass of the fragmented peptide; PEP, posterior error probability (probability of a false hit given the peptide identification score and length of peptides); UAKD, uromodulin-associated kidney diseases; wt, wild type. The mutated amino acid is highlighted in bold.

control, it is still adopting a nonnative conformation. ER quality control escape has already been observed for other disease-causing mutant proteins, for example, alpha-1-antitrypsin[18] and CFTR (cystic fibrosis transmembrane conductance regulator).[19] Interestingly, CFTR folding mutant ΔF508 on escape from the ER quality control is altering cellular lipid trafficking,[20] showing that misfolded proteins that gain access to the distal secretory pathway, in addition of being nonfunctional, can have a detrimental effect.

In the case of mutant uromodulin, this effect is evident in not only *in vitro* models but also *in vivo* models. Indeed, immunofluorescence analyses performed on kidney sections of a mouse model of UAKD ($Tg^{UmodC147W}$ mice) show intraluminal casts containing mutant uromodulin. These structures are an early finding in the mouse disease that can be found in virtually all TAL segments at time points (1 and 4 weeks of age) when renal function and nephron integrity are still preserved (Supplementary Figure S6 online and data not shown).

We believe that secretion of mutant uromodulin as seen in MDCK cells and in $Tg^{UmodC147W}$ mice is not merely due to overexpression. The relevance of these findings is indeed demonstrated by the detection of mutant uromodulin in the urine of three UAKD patients carrying three different mutations. Urinary mutant protein is likely derived from active protein secretion from the plasma membrane and not because of the presence of cell debris in the urine sample. Indeed, if that was the case, one would expect mutant uromodulin to be mainly present as the shorter ER-glycosylated isoform, which was never detected in western blots of patient urine. Mutant uromodulin was not found in the urine of UAKD patients in two earlier studies.[21,22] This discrepancy could be ascribed to the different *UMOD* mutations analyzed. However, it should be noticed that in both previous studies, uromodulin secretion was assessed at a time point when renal function of UAKD patients was already severely compromised. In this condition, total uromodulin secretion was highly reduced, possibly to such an extent to hamper the specific detection of mutant protein. In our experience, this was indeed the case in affected relatives of the patients analyzed in the current study who had reduced renal function (data not shown). This suggests that a mutation-specific effect is unlikely. Rather, mutant uromodulin secretion (ranging from ~1 to 30% of the wild-type protein level in our work) is evident in UAKD patients when renal function is still preserved.

What could be the consequences of extracellular mutant uromodulin aggregation? It is well known that uromodulin constitutes the matrix for the formation of hyaline casts.[23] Mutant uromodulin with its high propensity to aggregation could increase the number of hyaline casts formed in the TAL, leading to tubule obstruction, an event that could be upstream of inflammation and interstitial fibrosis. On a more speculative ground, we hypothesize that aggregation of mutant uromodulin could affect wild-type protein function by interfering with its polymerization or by sequestering it in large extracellular aggregates. This could affect the very recently described role of uromodulin in the regulation of water/salt balance in the TAL,[24] contributing to urinary concentrating defect and hyperuricemia in UAKD phenotype.

We believe that our findings have relevance when considering potential therapeutic strategies for UAKD, in particular the use of chemical chaperones to rescue mutant protein retention in the ER. The chemical chaperone sodium phenylbutyrate was shown to restore mutant uromodulin trafficking *in vitro*,[25] and the use of this drug has already been extensively tested for the treatment of other ER-storage disorders such as alpha-1 antitrypsin deficiency[26] or cystic fibrosis.[27] In the case of UAKD, chemical chaperones rescuing

intracellular retention would likely increase mutant protein delivery to the plasma membrane, thereby enhancing extracellular aggregation. We think that additional work would be needed to understand the potential negative consequences of such an effect that would be predicted to affect the TAL segment and kidney function.

In conclusion, our work shows that mutant uromodulin isoforms are secreted in the urine of patients with preserved renal function. Mutant uromodulin seems to have a higher propensity to aggregation than the wild-type protein because of either misfolding or different post-translational modification, for example glycosylation. The formation of extracellular casts could induce tubule obstruction, cast formation, and interfere with the function of wild-type uromodulin and possibly other membrane proteins. Thus, these data suggest that the proteotoxic effect of mutant uromodulin isoforms could be exerted through both intra- and extracellular gain-of-function mechanisms. This should be taken into account when envisaging therapeutic strategies for uromodulin-associated renal disorders.

MATERIALS AND METHODS

Uromodulin expression constructs

Wild-type uromodulin tagged with HA (pcDNA_HA_UMOD) was expressed from pcDNA 3.1(+) cloning vector (Invitrogen, Carlsbad, CA). Missense mutations were introduced in pcDNA_HA_UMOD by using the Quickchange mutagenesis kit (Stratagene, La Jolla, CA) following the manufacturer's instructions. Primers were designed using the software QuikChange Primer Design Program. For coexpression experiments, myc- or Flag-tagged and HA-tagged uromodulin isoforms were stably expressed from bicistronic vector pVITRO-hygro-mcs under the control of the elongation factor-1α promoter of mouse and rat, respectively (Invivogen, San Diego, CA). The HA, myc, or Flag tag was inserted after the leader peptide, in between T26 and S27 in the protein sequence as previously described.[28]

Cell line and culture condition

MDCK cells were grown in Dulbecco's modified Eagle's medium supplemented with 10% fetal bovine serum, 200 U/ml penicillin, 200 μg/ml streptomycin, and 2 mmol/l glutamine (complete medium) at 37 °C, 5% CO_2. Stable clones were generated by transfecting MDCK cells with Lipofectamine 2000 (Invitrogen) following the manufacturer's protocol. For pcDNA and pVITRO constructs, selection was started 24 h after transfection by adding 1 mg/ml G418 (Invitrogen) or 200 μg/ml hygromycin (Invitrogen), respectively, and was pursued for 2 weeks to obtain a population of resistant cells.

Tg^{Umod} mice and murine urine collection

Generation and characterization of Tg^{Umod} mice is described elsewhere.[13] Murine urine was obtained on age- and gender-matched transgenic and control mice (females, aged 10–12 weeks). They were housed in light- and temperature-controlled room with *ad libitum* access to water and standard chow. The 24-h urine collections were obtained at baseline in individual metabolic cages. All animal procedures were carried out at San Raffaele Scientific Institute (Milan, Italy) according to, and approved by, the San Raffaele Institutional Animal Care and Use Committee.

Patient and urine collection

Diagnostic criteria for patient collection and *UMOD* mutational screening procedures have been previously described.[6] Uromodulin was purified from 20 ml of urine as already reported,[3] and resuspended in distilled water. Purified protein was deglycosylated with PNGase F (New England Biolabs, Ipswich, MA) in denaturing/reducing conditions according to the manufacturer's instructions, alkylated in 55 mmol/l iodoacetamide or *N*-ethylmaleimide for 20 min at room temperature, separated on 8% acrylamide SDS–PAGE, and stained with Coomassie Brilliant Blue (Sigma–Aldrich, St Louis, MO).

Western blot

MDCK cells were grown to confluence. The complete medium was replaced with 2 ml of Opti-MEM (Invitrogen). After 24 h, the conditioned medium was collected, 4 volumes of acetone were added, and precipitated proteins were resuspended in 100 μl of phosphate-buffered saline. When indicated, cells were incubated with phosphatidylinositol-specific-PLC (PI-PLC) digestion medium (Dulbecco's modified Eagle's medium; 20 mmol/l Tris-HCl, pH 7.4; PI-PLC 0.3 U/ml; Invitrogen) for 3 h in a 5% $C0_2$ atmosphere at 37 °C. Cells were lysed in 300 μl of octylglucoside lysis buffer (50 mmol/l Tris-HCl, pH 7.4, 150 mmol/l NaCl, 60 mmol/l octyl-glucoside, and 1 mmol/l phenylmethylsulfonyl fluoride) for 1 h at 4 °C under rotation. Unsoluble fractions were resuspended in 50 μl of Laemmli buffer whereas soluble fractions were quantified by the Bio-Rad Protein Assay (Bio-Rad, Hercules, CA). When indicated, soluble fractions or PI-PLC digestion medium were deglycosylated with PNGase F or endoglycosidase H (New England Biolabs). A total of 30 μg of each protein lysate, 10 μl (1/5) of each unsoluble fraction, and 20 μl (1/5) of medium-precipitated proteins were loaded onto reducing 8% SDS–PAGE. Transblotted nitrocellulose membranes (GE Healthcare, Little Chalfont, Buckinghamshire, UK) were incubated with mouse monoclonal antibody against HA (1:2000 dilution; Covance Research Products, Princeton, NJ) or myc (1:1000 dilution; Covance), followed by incubation with horseradish peroxidase-conjugated secondary antibody (1:7500 dilution; GE Healthcare). Anti-α-tubulin mouse monoclonal antibody (1:1000 dilution; Santa Cruz Biotechnology, Santa Cruz, CA) and polyclonal anti-transferrin goat antibody (1:1000 dilution; Bethyl Laboratories, Montgomery, TX) were used as a loading control for lysate and precipitated medium, respectively. Protein bands were visualized with the Immobilon Western Chemiluminescent Horseradish Peroxidase Substrate kit (Millipore, Billerica, MA).

Sucrose gradient

PI-PLC digestion medium was overlaid on a discontinuous gradient consisting of 1, 1.5, and 2 M sucrose in Dulbecco's modified Eagle's medium and centrifuged at 100,000 *g* for 2 h. After centrifugation, the gradient was separated in six fractions that were precipitated with acetone and analyzed by western blot using a sheep anti-uromodulin antibody (1:1000 dilution; Abcam, Cambridge, UK).

Immunoprecipitation

MDCK cells grown to confluence (3 dishes 100 mm/line) were kept for 30 h in Opti-MEM (Invitrogen). The conditioned medium was collected, pooled, and concentrated on Amicon-Ultra-15 3K (Millipore) to obtain a total volume of 700 μl. A total of 500 μl of the concentrated medium was added to 40 μl of anti-Flag M2 affinity gel (Sigma-Aldrich). After an overnight incubation at 4 °C under rotation, the resin was washed three times with 1 ml

phosphate-buffered saline, resuspended in 60 µl Laemmli buffer, and boiled. Then, 50 µl of the concentrated medium and 30 µl of the immunoprecipitate were loaded on SDS–PAGE and analyzed by western blot as described above using a rabbit anti-Flag antibody (1:2000 dilution; Sigma-Aldrich) or a mouse anti-HA antibody (1:1000 dilution; Covance).

Immunofluorescence

Cells grown on coverslip in 12-well plate were fixed in 4% paraformaldehyde for 30 min. When needed, cells were permeabilized for 10 min at room temperature with 0.5% Triton X-100. Cells were labeled for 1 h and 30 min at room temperature with anti-HA (1:500; Covance) and anti-myc (1:500; Novus Biologicals, Littleton, CO) and anti-calnexin (dilution 1:500; Sigma–Aldrich) antibodies. After incubation with the appropriate secondary antibody (1:500; Invitrogen), cells were stained with 4,6-diamidino-2-phenylindole and mounted using FluorSave Reagent (Calbiochem, San Diego, CA).

To collect renal tissue, animals were anesthetized with avertin and perfused with a 4% paraformaldehyde solution. Kidneys were taken and fixed in 4% paraformaldehyde solution for additional 16 h and embedded in optimum cutting temperature embedding medium (Tissue-Tek, Electron Microscopy Sciences, Hatfield, PA), snap-frozen in a mixture of isopentane and dry ice, and stored at −80 °C. Immunofluorescence was carried out on tissue sections (10 µm thick) stained with rat anti-HA antibody (Roche, Indianapolis, IN) and anti-NKCC2 antibody (kind gift from Professor Sebastian Bachmann, Charité University, Berlin, Germany).

All slides were visualized under a DM 5000B fluorescence upright microscope (Leica DFC480 camera, Leica DFC Twain Software, 40X/0.75 lens; Leica Microsystems, Deerfield, IL) or with an UltraVIEW ERS spinning disk confocal microscope (UltraVIEW ERS-Imaging Suite Software, Zeiss 63X/1.4; PerkinElmer Life and Analytical Sciences Boston, MA). All images were imported in Photoshop CS (Adobe Systems, Mountain View, CA) and adjusted for brightness and contrast.

The area of polymers covering the plasma membrane in cells coexpressing myc-tagged wild-type uromodulin together with either wild-type or mutant HA-tagged protein was quantified using Image J software (http://imagej.nih.gov/ij/) (Supplementary Figure S7 online). The analysis was performed on pictures taken at ×10 magnification that were adjusted for brightness and contrast and after setting a threshold to exclude the membrane signal background. Only polymers positive for both tags were quantified by setting a selection mask on the HA channel and restoring it on the myc one. The selected area was quantified by setting an object size limit of 300 pixels. For each experiment, ~1000 objects were quantified per line. Data are expressed as average ± SEM and compared by unpaired two-tailed *t*-test analysis (Prism software; GraphPad, San Diego, CA).

MS analysis

Liquid chromatography–tandem MS (LC–MS/MS) analysis. Bands of interest were excised from gels of patients, subjected to reduction by 10 mmol/l dithiothreitol and alkylation by 55 mmol/l iodoacetamide or *N*-ethylmaleimide, and finally digested overnight with trypsin (Roche).[29] After acidification, up to 10% formic acid, peptide mixtures were concentrated and desalted on StageTips µC18 (Proxeon Biosystem, Odense, Denmark)[30] and injected in a capillary chromatographic system (EasyLC, Proxeon Biosystem). Peptide separations occurred on a RP homemade 15 cm reverse-phase spraying fused silica capillary column (75 µm i.d. × 15 cm), packed with 3 µm ReproSil-Pur C18-AQ (Dr Maisch GmbH, Ammerbuch-Entringen, Germany). A gradient of eluents A (H_2O with 2% v/v acetonitrile, 0.5% v/v acetic acid) and B (80% acetonitrile with 0.5% v/v acetic acid) was used to achieve separation, from 7% B (at 0 min, 0.2 µl/min flow rate) to 35% B (in 70 min, 0.2 µl/min flow rate). The LC system was connected to an LTQ-Orbitrap mass spectrometer (Thermo Fisher Scientific, Waltham, MA) equipped with a nanoelectrospray ion source (Proxeon Biosystems). MS and MS/MS spectra were acquired selecting the 10 most intense ions per survey spectrum acquired in the orbitrap from *m*/*z* 300–1750 with 60,000 resolution. Target ions selected for the MS/MS were fragmented in the ion trap and dynamically excluded for 45 s. Target value were 1,000,000 for survey scan and 100,000 for MS/MS scan. For accurate mass measurements, the lock-mass option was employed.[31]

Data processing and analysis. For peptide identifications, Mascot (Matrix Science, version 2.2.07, Boston, MA) search engine was used. Raw MS files were converted into peaklist (.msm files), and searched against the database IPI_human_20100628 (86,397 sequences; 35,097,130 residues) supplemented with the on-purpose-created sequences of human uromodulin variants with mutations R212C (IPI99999999), C256Y (IPI99999996), and C317Y (IPI99999995).

Enzyme specificity was set to trypsin, allowing a maximum of two missed cleavages. Cysteine alkylation by iodoacetamide or *N*-ethylmaleimide or acrylamide, oxidation of methionine, deamidation of asparagines, and protein *N*-acetylation were all considered as variable modifications. Mass tolerance was set to 5 p.p.m. and 0.6 Da for precursor and fragment ions, respectively. The criterion used to evaluate the quality of MS/MS data was a Mascot ion score cutoff of at least 20.

Data analysis by MaxQuant. To measure the intensity of peptides, especially the intensity of the mutated peptides and the correspondent wild-type peptides in each sample from urine of patients, MS data were analyzed using the MaxQuant software,[32,33] version 1.1.1.25, applying the Label-free algorithms.

For MS/MS peak list file construction, up to top 6 peaks per 100 Da window were included for database searching. The generated peak lists were searched against the concatenated forward and reverse database IPI_human_20100628 (86,397 sequences; 35,097,130 residues) supplemented with the on-purpose-created sequences of human uromodulin variants with mutations R212C (IPI99999999), C256Y (IPI99999996), and C317Y (IPI99999995). Mass tolerance was set to 7 p.p.m. and 0.6 Th for precursor and fragment ions, respectively. Cysteine alkylation by iodoacetamide or *N*-ethylmaleimide and acrylamide, protein N-terminal acetylation, asparagine deamidation, and methionine oxidation were set as variable modifications for the database search. The cutoff false discovery rate for proteins and peptides was set to 0.01, and peptides with a minimum of six amino acids were considered for identification. The derived peptides intensities were used for a rough estimation of relative peptide abundances.

DISCLOSURE

All the authors declared no competing interests.

ACKNOWLEDGMENTS

We are grateful to Emanuele Alpi for in-house Mascot modifications and Max Quant applications. We thank Cesare Covino for technical assistance on the quantification of polymer area. This work was supported by Telethon-Italy (TCR08006) and the European Community's 7th Framework Program (HEALTH-F2-2007-201590, EUNEFRON program). LR is an Associate Telethon Scientist.

SUPPLEMENTARY MATERIAL

Figure S1. Western-blot analysis of HA-tagged uromodulin released after PLC cleavage from MDCK cell plasma membrane and deglycosylated with PNGase F or EndoH; control, untreated sample.
Figure S2. Western-blot analysis of uromodulin from MDCK cells expressing myc-tagged wild-type and either wild-type or mutant HA-tagged isoforms. Both uromodulin present in the cell lysate (top row) and secreted in the medium (bottom row) are shown. Tubulin and transferrin are shown as loading controls.
Figure S3. MS/MS spectra of the wild-type peptide (**a**) and the correspondent mutated peptide (**b**) obtained by analysis of uromodulin purified from the urine of patient with R212C mutation.
Figure S4. MS/MS spectra of the wild-type peptide (**a**) and the correspondent mutated peptide (**b**) obtained by analysis of uromodulin purified from the urine of patient with C256Y mutation.
Figure S5. MS/MS spectra of the wild-type peptide (**a**) and the correspondent mutated peptide (**b**) obtained by analysis of uromodulin purified from the urine of patient with C317Y mutation.
Figure S6. Immunofluorescence performed on kidney sections of Tg^{Umodwt} and $Tg^{UmodC147W}$ mice at 1 week of age showing transgenic HA-tagged uromodulin. Uromodulin aggregates are present exclusively in TAL lumen of $Tg^{UmodC147W}$ mice. Bar = 25 μm.
Figure S7. Representative pictures for the quantification of polymer average area on unpermeabilized MDCK cells expressing myc-tagged wild-type and either wild-type or mutant (C317Y) HA-tagged uromodulin isoforms. Top row: merged myc (green) and HA (red) signal. Bottom row: selection outline defining quantified areas. Bar = 100 μm.
Supplementary material is linked to the online version of the paper at http://www.nature.com/ki

REFERENCES

1. Tamm I, Horsfall FL. Characterisation and separation of an inhibitor of viral hemagglutination present in urine. *Proc Soc Exp Biol Med* 1950; **74**: 108–114.
2. Bachmann S, Koeppen-Hagemann I, Kriz W. Ultrastructural localization of Tamm-Horsfall glycoprotein (THP) in rat kidney as revealed by protein A-gold immunocytochemistry. *Histochemistry* 1985; **83**: 531–538.
3. Santambrogio S, Cattaneo A, Bernascone I *et al.* Urinary uromodulin carries an intact ZP domain generated by a conserved C-terminal proteolytic cleavage. *Biochem Biophys Res Commun* 2008; **370**: 410–413.
4. Serafini-Cessi F, Malagolini N, Cavallone D. Tamm-Horsfall glycoprotein: biology and clinical relevance. *Am J Kidney Dis* 2003; **42**: 658–676.
5. Hart TC, Gorry MC, Hart PS *et al.* Mutations of the UMOD gene are responsible for medullary cystic kidney disease 2 and familial juvenile hyperuricaemic nephropathy. *J Med Genet* 2002; **39**: 882–892.
6. Rampoldi L, Caridi G, Santon D *et al.* Allelism of MCKD, FJHN and GCKD caused by impairment of uromodulin export dynamics. *Hum Mol Genet* 2003; **12**: 3369–3384.
7. Lens XM, Banet JF, Outeda P *et al.* A novel pattern of mutation in uromodulin disorders: autosomal dominant medullary cystic kidney disease type 2, familial juvenile hyperuricemic nephropathy, and autosomal dominant glomerulocystic kidney disease. *Am J Kidney Dis* 2005; **46**: 52–57.
8. Scolari F, Caridi G, Rampoldi L *et al.* Uromodulin storage diseases: clinical aspects and mechanisms. *Am J Kidney Dis* 2004; **44**: 987–999.
9. Bernascone I, Vavassori S, Di Pentima A *et al.* Defective intracellular trafficking of uromodulin mutant isoforms. *Traffic* 2006; **7**: 1567–1579.
10. Vylet'al P, Kublova M, Kalbacova M *et al.* Alterations of uromodulin biology: a common denominator of the genetically heterogeneous FJHN/MCKD syndrome. *Kidney Int* 2006; **70**: 1155–1169.
11. Jennings P, Aydin S, Kotanko P *et al.* Membrane targeting and secretion of mutant uromodulin in familial juvenile hyperuricemic nephropathy. *J Am Soc Nephrol* 2007; **18**: 264–273.
12. Williams SE, Reed AA, Galvanovskis J *et al.* Uromodulin mutations causing familial juvenile hyperuricaemic nephropathy lead to protein maturation defects and retention in the endoplasmic reticulum. *Hum Mol Genet* 2009; **18**: 2963–2974.
13. Bernascone I, Janas S, Ikehata M *et al.* A transgenic mouse model for uromodulin-associated kidney diseases shows specific tubulo-interstitial damage, urinary concentrating defect and renal failure. *Hum Mol Genet* 2010; **19**: 2998–3010.
14. Scolari F, Puzzer D, Amoroso A *et al.* Identification of a new locus for medullary cystic disease, on chromosome 16p12. *Am J Hum Genet* 1999; **64**: 1655–1660.
15. Jovine L, Qi H, Williams Z *et al.* The ZP domain is a conserved module for polymerization of extracellular proteins. *Nat Cell Biol* 2002; **4**: 457–461.
16. Ksiezak-Reding H, Wall JS. Mass and physical dimensions of two distinct populations of paired helical filaments. *Neurobiol Aging* 1994; **15**: 11–19.
17. de Godoy LM, Olsen JV, Cox J *et al.* Comprehensive mass-spectrometry-based proteome quantification of haploid versus diploid yeast. *Nature* 2008; **455**: 1251–1254.
18. Miranda E, Perez J, Ekeowa UI *et al.* A novel monoclonal antibody to characterize pathogenic polymers in liver disease associated with alpha1-antitrypsin deficiency. *Hepatology* 2010; **52**: 1078–1088.
19. Hegedus T, Aleksandrov A, Cui L *et al.* F508del CFTR with two altered RXR motifs escapes from ER quality control but its channel activity is thermally sensitive. *Biochim Biophys Acta* 2006; **1758**: 565–572.
20. Gentzsch M, Choudhury A, Chang XB *et al.* Misassembled mutant DeltaF508 CFTR in the distal secretory pathway alters cellular lipid trafficking. *J Cell Sci* 2007; **120**: 447–455.
21. Dahan K, Devuyst O, Smaers M *et al.* A cluster of mutations in the UMOD gene causes familial juvenile hyperuricemic nephropathy with abnormal expression of uromodulin. *J Am Soc Nephrol* 2003; **14**: 2883–2893.
22. Rezende-Lima W, Parreira KS, Garcia-Gonzalez M *et al.* Homozygosity for uromodulin disorders: FJHN and MCKD-type 2. *Kidney Int* 2004; **66**: 558–563.
23. Wenk RE, Bhagavan BS, Rudert J. Tamm-Horsfall uromucoprotein and the pathogenesis of casts, reflux nephropathy, and nephritides. *Pathobiol Annu* 1981; **11**: 229–257.
24. Renigunta A, Renigunta V, Saritas T *et al.* Tamm-Horsfall glycoprotein interacts with renal outer medullary potassium channel ROMK2 and regulates its function. *J Biol Chem* 2011; **286**: 2224–2235.
25. Choi SW, Ryu OH, Choi SJ *et al.* Mutant Tamm-Horsfall glycoprotein accumulation in endoplasmic reticulum induces apoptosis reversed by colchicine and sodium 4-phenylbutyrate. *J Am Soc Nephrol* 2005; **16**: 3006–3014.
26. Burrows JA, Willis LK, Perlmutter DH. Chemical chaperones mediate increased secretion of mutant alpha 1-antitrypsin (alpha 1-AT) Z: a potential pharmacological strategy for prevention of liver injury and emphysema in alpha 1-AT deficiency. *Proc Natl Acad Sci USA* 2000; **97**: 1796–1801.
27. Rubenstein RC, Zeitlin PL. A pilot clinical trial of oral sodium 4-phenylbutyrate (Buphenyl) in deltaF508-homozygous cystic fibrosis patients: partial restoration of nasal epithelial CFTR function. *Am J Respir Crit Care Med* 1998; **157**: 484–490.
28. Schaeffer C, Santambrogio S, Perucca S *et al.* Analysis of uromodulin polymerization provides new insights into the mechanisms regulating ZP domain-mediated protein assembly. *Mol Biol Cell* 2009; **20**: 589–599.
29. Shevchenko A, Wilm M, Vorm O *et al.* Mass spectrometric sequencing of proteins silver-stained polyacrylamide gels. *Anal Chem* 1996; **68**: 850–858.
30. Rappsilber J, Mann M, Ishihama Y. Protocol for micro-purification, enrichment, pre-fractionation and storage of peptides for proteomics using StageTips. *Nat Protoc* 2007; **2**: 1896–1906.
31. Olsen JV, de Godoy LM, Li G *et al.* Parts per million mass accuracy on an Orbitrap mass spectrometer via lock mass injection into a C-trap. *Mol Cell Proteomics* 2005; **4**: 2010–2021.
32. Cox J, Mann M. MaxQuant enables high peptide identification rates, individualized p.p.b.-range mass accuracies and proteome-wide protein quantification. *Nat Biotechnol* 2008; **26**: 1367–1372.
33. Cox J, Matic I, Hilger M *et al.* A practical guide to the MaxQuant computational platform for SILAC-based quantitative proteomics. *Nat Protoc* 2009; **4**: 698–705.